# Crystallization Rates of Matched Fractions of $MgCl_2$-Supported Ziegler-Natta and Metallocene Isotactic Poly(propylene)s. 2. Chain Microstructures from a Supercritical Fluid Fractionation of a $MgCl_2$-Supported Ziegler−Natta Isotactic Poly(propylene)†

**James C. Randall***

*2710 Ridge Road, Steamboat Springs, Colorado 80487*

**Rufina G. Alamo**

*Department of Chemical Engineering, Florida Agricultural and Mechanical University and Florida State University, Tallahassee, Florida 32310-6046*

**Pawan K. Agarwal and Charles J. Ruff**

*Baytown Polymers Center, Exxon Chemical Company, 5200 Bayway Drive, Baytown, Texas 77522-5200*

*Received October 3, 2002; Revised Manuscript Received December 24, 2002*

ABSTRACT: Two and three-state statistical models, which are mathematical devices used to partition observed poly(propylene) sequence distributions, are usually evaluated on how well they reproduce observed overall pentad/heptad distributions from $^{13}C$ NMR. In this study, sequence distribution curves vs crystallization rates are also employed to judge the behavior of a particular model. A supercritical fluid fractionation of a poly(propylene) prepared with a $MgCl_2$-supported Ziegler−Natta catalyst provided a series of samples that had progressively decreasing *racemic* contents as the molar masses increased. A modification was made to an existing three-state statistical model that gave sequence distribution curves that satisfied the fractionation behavior as well as linear spherulitic growth rates and polymorphic behaviors observed for the series of Ziegler−Natta poly(propylene) fractions. The results indicate that $MgCl_2$-supported Ziegler−Natta isotactic poly(propylene)s contain significant amounts of a high molar mass, extremely isotactic poly(propylene) molecules with average isotactic sequence lengths exceeding a thousand or more. There is a second predicted major type of polypropylene molecule, which has some isotactic blocks of opposite handedness, an average isotactic sequence length of around 200 and a sequence length distribution curve that partially overlaps with that of the highly isotactic component. Finally, a third and minor component is a stereoblock type of poly(propylene) molecule, which has an average isotactic sequence length of no more than 5−25 repeat units. This microstructural distribution, predicted by the newly modified three-state statistical model, is also consistent with that reported in the literature for a similar $MgCl_2$-supported Ziegler−Natta poly(propylene) where the intermolecular microstructural distribution was derived from a TREF study.

## Introduction

It is well-known that fourth-generation $MgCl_2$-supported Ziegler−Natta catalysts used in the production of isotactic poly(propylene)s are multisited. This behavior leads to a complex and varied intermolecular distribution of poly(propylene) microstructures. Accompanying a predominantly isotactic poly(propylene) component are atactic poly(propylene)s, stereoblock poly(propylene)s and some predominantly syndiotactic structures.[1−4] The distribution among these structures is related to the overall *meso* diad content.[3,4] When catalyst recipes are modified to increase the overall *meso* diad content, the isotactic fraction increases in both amount and average isotactic sequence length while the atactic, stereoblock, and syndiotactic contents are suppressed.[3,4]

Carbon-13 NMR has been useful in the analysis of the distribution of the various types of poly(propylene) structures because a pentad/heptad sensitivity is routinely available in the methyl region from spectrometers operating in the 75−150 MHz range for $^{13}C$ nuclei. Some important resonances are *mmmm* (isotactic pentad), *mmmr* (connecting pentad to any stereodefect), *mmrrmm* (heptad for a single stereo inversion), *mmrrrm* (heptad with a short syndiotactic block connecting meso diads of opposite handedness), and *rrrrrr* (a syndiotactic heptad). All of these resonances are found in $^{13}C$ NMR spectra of crystalline fractions obtained from highly isotactic poly(propylene)s[1−3,5] prepared with $MgCl_2$-supported Ziegler−Natta catalyst systems.

There have been a number of attempts to decipher the structural distributions characteristic of classical Ziegler−Natta isotactic poly(propylene)s by applying two and three-state statistical models to normalized pentad/heptad/nonad distributions obtained from $^{13}C$ NMR. The first two-state model, proposed independently by Chûjô[6] and Doi,[7] was developed to predict a simple mixture of asymmetric and symmetric poly(propylene) chains. The concept of asymmetric and symmetric chains, which arises from Markovian statistics, was first introduced by Price.[8] A requirement for a poly(propylene) asymmetric chain is that one of two

* Corresponding author. E-mail: jimschrada@aol.com.

† Dedicated to Prof. L. Mandelkern on the occasion of his 80th birthday.

10.1021/ma021550f CCC: $25.00 
Published on Web 02/14/2003

possible transition probabilities must be dominant, that is, $P_0 \gg P_1$, where $P_0$ is the probability of a particular configuration ("0") and $P_1$ is the probability of its opposite configuration ("1").[9] Asymmetric chains are typically associated with poly(propylene)s produced from catalysts exhibiting enantiomorphic site (Es) control. In such cases, the catalyst controls the configuration and there is no effect from the configuration created by a previous monomer insertion. It is therefore natural for both Chûjô and Doi to utilize random asymmetric chain statistics to describe one of the states in their original two-state model.

The second component in the original two-state model utilized symmetric chain statistics, which were often discussed by Bovey [10,11] and are sometimes called the Bovey model. A property of symmetric chain statistics is that $P_0 = P_1$. This leads to the relationships $P_{00} = P_{11} = P_m$ and $P_{01} = P_{10} = P_r$. Poly(propylene) symmetric chain statistics are usually associated with Ziegler−Natta catalyst sites that exhibit "chain-end control" (CE) where there is the possibility that the nature of a previous monomer insertion will determine how a new monomer inserts, but the overall populations of the two types of insertions are the same. Symmetric chains are also associated with free radical and alkyllithium polymerizations, such as in the case of polystyrene, where repeat unit configurations occur randomly.[12,13] The original Chûjô/Doi two-state model used random symmetric chain statistics to account for atactic and stereoblock components observed in isotactic poly(propylene)s made with Ziegler−Natta catalysts.

There have been a number of variations and modifications to the Chûjô/Doi two-state models in attempts to identify the range of structures of isotactic poly(propylene)s produced with modern, $MgCl_2$-supported Ziegler−Natta catalysts.[1−3,5] The most notable two-state modifications were suggested by Busico et al.[2] In his two-state model, Busico proposed that an asymmetric chain component could be produced by monomer insertions moving back and forth between two enantiomorphic control sites (*C1*). He introduced the probabilities of growth at each site and the probabilities of moving from site 1 to site 2 and vice versa. His CE symmetric chain component was the same as that given by Chûjô/Doi. In his three-state model, Busico[2] simply added back a single site, enantiomorphic control component (Es) to his above two-state model. By doing this, Busico was able to account for the pentad/heptad/nonad sequence distributions observed for a late generation, but weakly isotactic, Ziegler−Natta poly(propylene).[2]

The present investigation reports results from fitting experimental $^{13}C$ NMR pentad/heptad distributions with an improved three-state statistical model on a series of poly(propylene)s, obtained after a fractionation of a $MgCl_2$-supported Ziegler−Natta highly isotactic poly(propylene). The fractions were partitioned by molar mass in a supercritical fluid fractionation where it was observed that the overall levels of stereodefects decreased with increasing molecular weight.[14]

Corresponding fractions from a matching isotactic poly(propylene) produced with a metallocene catalyst were also examined.[14] The application of models in the metallocene case is straightforward because only one state describing asymmetric chains produced by enantiomorphic site control[15] is required. Uniform defect levels were observed in each of the fractions independently of molecular weight, as expected for an isotactic poly(propylene) produced from a single sited catalyst yielding a product with uniform composition and molecular weight distributions.[16] For isotactic metallocene poly(propylene)s, the use of either an Es state or an alternating state leads to the same result.[15]

Another topic of exceptional interest is whether poly(propylene) sequence or defect distributions are nonrandom, either on an intramolecular or intermolecular basis, as could be suggested by the linear spherulitic growth rates and polymorphic behavior discussed in the first paper of this series.[14] Generally, attempts to apply two-state and three-state models to predict recently observed pentad/heptad/nonad sequence distributions employ statistics where each of the states are defined with random (Bernoullian) parameters.[1,2,6,7] A pentad/heptad/nonad sequence distribution fit with random statistics using a two- or three-state model infers not only that the stereodefects are randomly situated among all chains but also that the different types of poly(propylene) molecules have narrow compositional distributions, independently of molar mass. The latter point is not often considered in the design of two- and three-state models.[17] Random statistics are the statistics of choice for the Es and *C1* states because these chains are produced by enantiomorphic site control. Use of higher order Markovian statistics for either the Es or *C1* states would only be employed to address a problem of broad compositional distributions. It has been demonstrated that a mixture of random chains having different compositions combine to form an average distribution that is nonrandom.[18,19] For Ziegler−Natta catalysis, where there is a broad distribution of catalyst sites, the final blend of polymers is characterized by a nonrandom distribution, even though each catalyst site may be acting independently to produce poly(propylene)s with randomly distributed stereodefects.

The two- and three-state models are useful for addressing fundamental differences in catalyst site behavior, but the problem of a broad compositional distribution within a given state is not handled by simple random statistics. To address the problem of overall nonrandom distributions created by broad compositional distributions for a particular type of catalyst site, some investigators have chosen first-order Markovian statistics for at least the symmetric chain component.[3,20] This problem can also be corrected by using a Coleman−Fox two-state model[21] for the symmetric chain component in a two- or three-state model.[20] It has been shown recently that first-order Markovian statistics also reasonably predict an overall sequence distribution for a mixture of two or more random components.[22] Certainly, first-order Markovian statistics offer a good choice for symmetric chains produced by chain-end control (CE1). This will allow an opportunity for this component to have a broad compositional distribution, in addition to offering a better approach from a mechanistic point of view. In an earlier study, the use of first-order Markovian statistics for the Es component led to a result where the system automatically reverted to the Bernoullian case, because $P_{10} \approx P_{00}$ and $P_{01} \approx P_{11}$[3]. This result suggests intrinsically that the Es sites lead to poly(propylene)s with fairly narrow compositional distributions. The downside of using higher order Markovian statistics in any particular state is that another unknown is added to a two- or three-state model, which is then better tested with a large databank.

After considering the complexity of Ziegler−Natta poly(propylene)s, it is surprising that so many good fits are reported with simple two- and three-state models.[1−3,6,7,20] Results from any two- or three-state model analysis using $^{13}C$ NMR data are based upon fitting an observed pentad/heptad distribution from an "average molecule", which represents a sum over all of the molecules in the sample. A fit is determined after iterations over various model parameters lead to a minimum in the standard deviation between a calculated and observed pentad/heptad/nonad distribution. The fits are not perfect, but do fall within experimental error of the measurements.[1−3,6,7,20] The consistency of these results suggests that the compositional distributions within the various states must be fairly narrow. Nonrandom behavior, associated with broad composition distributions within the individual component states, would have to be detected by reproducible deviations between experimental and calculated results after using simple, random statistics for the individual states. Presumably, with the proper experimental precision, any departures from a random fit by an observed distribution could be attributed to nonrandom behavior of the component states. The quality of the present fits indicate that a higher level of precision in the NMR measurements, than is currently possible, would be required to ascertain nonrandom behavior associated with broad composition distributions within the given states. This is a major consequence of the very low defect concentrations found in highly isotactic poly(propylene)s prepared with industrial $MgCl_2$-supported Ziegler−Natta catalysts, as well as the possibility that the individual component states do not exhibit exceedingly broad composition distributions.

Up to this point, we have been concerned only with intermolecular variations in compositions of individual random chains. As discussed above, random chains add to form a nonrandom distribution if they have different random compositions. The problem of detecting intramolecular nonrandom sequence distributions is far more difficult. Present two- and three-state model fits are based on sets of sequence distributions that are very short. At best, information from only up to a nonad distribution has been included in analyses of two- and three-state statistical models.[2] It would be desirable to have longer sequences than presently detected by $^{13}C$ NMR to detect intramolecular nonrandom sequence distributions. In $^{13}C$ NMR data, it is impossible to distinguish stereodefects that terminate contiguous isotactic sequences of 10 units from those that connect isotactic sequences of 100 units or more. Any inference of a nonrandom intramolecular distribution of stereodefects would best rely upon independent physical evidence outside of $^{13}C$ NMR. With improvements in the sensitivity of NMR measurements, contributions from intramolecular, nonrandom behavior to average sequence length distributions may some day be determined. For the time being, because of the limited sequence length data available from $^{13}C$ NMR, we have to be satisfied with results from pentad/heptad or nonad statistical fits that utilize either Bernoullian or first-order Markovian statistics.

The present study was undertaken because a series of samples from a fractionated Ziegler−Natta isotactic poly(propylene) (ZN iPP) were available where the defect concentrations decreased as the molar masses increased. The fractionation provided an opportunity to test the feasibility of various two- and three-state statistical models on a series of fractions, as opposed to a single analysis on a whole polymer. Important crystallization and thermal data were also available on each of the fractions, which would help establish if the samples had random defect distributions.[14] Last, statistical fits utilizing either two- or three-state models would permit structural trends, which were then examined for consistency with the crystallization and fractionation data, to be established as the fractions progressed in molecular weight with decreasing defect concentrations. This broadly based evaluation increases the confidence in results obtained with any particular two- or three-state statistical model.

A new scheme for evaluating the quality of two- and three-state models is employed for the first time in this study, that is, the transition probabilities obtained from each component in the two- and three-state models were used to calculate sequence distribution curves. This ingredient has been missing from previous analyses of two-state and three-state statistical models of $^{13}C$ NMR pentad/heptad/nonad distributions.[1−3,6,7,20] This new approach provides an opportunity to evaluate the models in light of the crystallization data and lends support to the use of first-order Markovian statistics for the symmetric chain component in the Busico three-state model. It is interesting to observe how the characteristics of the sequence distribution curves for the various states in the two- and three-state models differ for component states. Simple comparisons of experimental vs calculated pentad/heptad distributions do not reveal the necessary type of information required for evaluating crystallization data. It is important to establish both the peaks and the breadths of component sequence distribution curves. For evaluation purposes, it is also necessary to determine how the sequence length distribution curves from the same states in the various two- and three-state models vary from fraction to fraction with increasing molar mass. Only then can a particular two- or three-state model be properly evaluated for consistency with independently determined crystallization data.

Poly(propylene)s can be properly viewed as copolymers of *meso* and *racemic* propylene diads. The defects interrupting long blocks of isotactic sequences will be composed of one or more *racemic* pairs. Theoretical accounts of the crystallization and melting of these "copolymers" have been undertaken from phase equilibrium considerations involving more than one species.[23] When defects are rejected from the crystal, the equilibrium melting/crystallization temperature does not depend directly on the composition of the copolymer but rather upon the sequence distribution. The sequence distribution probability of a block copolymer is one. This requires that there is no depression in the melting or crystallization of block copolymers with increasing lengths or numbers of blocks. Equilibrium models also add restrictions on the length of the crystallizable sequences at any given temperature. Only sequences above a critical length can participate in the crystallization.[23] There are, however, kinetic considerations during isothermal crystallization in the selection of all sequences above a critical required length. This rate of selection is a function of the length and availability of a given sequence. Copolymers with differences in the concentration of defects or in the sequence distribution of the crystallizable units will show differences in their

**Table 1. Experimental vs Calculated Results for Various Two-State and Three-State Models for Zf97K1.03**

| | obsd | Es/CE | Es/CE1 | *C1*/CE | *C1*/CE1 | Es/*C1*/CE | Es/*C1*/CE1 |
|---|---|---|---|---|---|---|---|
| | | | | Pentad/Heptad | | | |
| *mmmm* | 0.9357 | 0.9358 | 0.9356 | 0.9358 | 0.9356 | 0.9357 | 0.9355 |
| *mmmr* | 0.0205 | 0.0193 | 0.0202 | 0.0193 | 0.0202 | 0.0196 | 0.0204 |
| *rmmr* | 0.0016 | 0.0006 | 0.0008 | 0.0006 | 0.0008 | 0.0009 | 0.0007 |
| *mmrr* | 0.0200 | 0.0200 | 0.0194 | 0.0200 | 0.0194 | 0.0198 | 0.0194 |
| *mmrm* + *rrmr* | 0.0036 | 0.0040 | 0.0039 | 0.0040 | 0.0039 | 0.0043 | 0.0038 |
| *rmrm* | 0.0008 | 0.0012 | 0.0007 | 0.0012 | 0.0007 | 0.0017 | 0.0014 |
| *mrrrrm* | 0.0013 | 0.0004 | 0.0006 | 0.0004 | 0.0006 | 0.0007 | 0.0008 |
| *mrrrrr* | 0.0016 | 0.0020 | 0.0026 | 0.0020 | 0.0026 | 0.0010 | 0.0020 |
| *rrrrrr* | 0.0036 | 0.0034 | 0.0032 | 0.0034 | 0.0032 | 0.0037 | 0.0035 |
| *rmrrrm* | 0.0000 | 0.0006 | 0.0003 | 0.0006 | 0.0003 | 0.0002 | 0.0001 |
| *rrrrmr* | 0.0016 | 0.0020 | 0.0007 | 0.0020 | 0.0007 | 0.0010 | 0.0001 |
| *mmrrrr* + *mmrrrm* | 0.0023 | 0.0009 | 0.0042 | 0.0009 | 0.0042 | 0.0015 | 0.0042 |
| *rmrrmr* | 0.0000 | 0.0003 | 0.0000 | 0.0003 | 0.0000 | 0.0001 | 0.0000 |
| *rmrrmm* | 0.0014 | 0.0004 | 0.0004 | 0.0004 | 0.0004 | 0.0013 | 0.0011 |
| *mmrrmm* | 0.0062 | 0.0093 | 0.0074 | 0.0093 | 0.0074 | 0.0085 | 0.0070 |
| std dev | | 0.0011 | 0.0006 | 0.0011 | 0.0006 | 0.0008 | 0.0008 |
| | | | | Triad/Diad | | | |
| *mm* | 0.958 | 0.956 | 0.957 | 0.956 | 0.957 | 0.956 | 0.957 |
| *mr* + *rm* | 0.024 | 0.025 | 0.024 | 0.024 | 0.024 | 0.026 | 0.024 |
| *rr* | 0.018 | 0.019 | 0.019 | 0.019 | 0.019 | 0.018 | 0.019 |
| *m* | 0.970 | 0.968 | 0.969 | 0.968 | 0.969 | 0.969 | 0.969 |
| *r* | 0.030 | 0.032 | 0.031 | 0.031 | 0.031 | 0.031 | 0.031 |
| $N_m$ | 80 | 77 | 81 | 79 | 81 | 75 | 80 |
| MRL | 91 | 97 | 92 | 97 | 92 | 95 | 91 |

crystallization rates. Poly(propylene) components that have short sequence distributions are not likely to contribute to the crystallization behavior, which conversely, should relate primarily to isotactic poly(propylene) components with sequence distributions over very long sequence lengths. Thus, sequence distributions predicted by a satisfactory model should be consistent with observed crystallization behavior.[14] The trends in sequence distribution curves, predicted successively for each fraction by the improved Busico three-state model, follow consistent patterns and are, at the same time, consistent with the crystallization data. This greatly increases our confidence in the results. It would be difficult to conclude that a unique solution is obtained with a complex three-state model from any single pentad/heptad analysis.

## Experimental Section

Experimental details for measurements of overall crystallization rates, linear spherulitic growth rates, $^{13}$C NMR, GPC, and the supercritical fluid fractionation have been given in the first part of this series.[14] The $^{13}$C NMR heptad assignments used in this study are from Busico et al.,[24] where the following heptads had been re-assigned from those presented in an earlier study:[1]

| | |
|---|---|
| 20.17 ppm | *rmrrrm* → *rmrrrm* |
| 20.13 ppm | *rrrrmr* + *mmrrrm* → *rrrrmr* |
| 20.06 ppm | *mmrrrr* → *mmrrrm* + *mmrrrr* |

The other pentad/heptad assignments remain unchanged from the earlier study. After evaluating both sets of assignments, we found that the new assignments had no significant effect upon the overall fits because of the very low concentrations for these particular *mrrr*-centered heptads. The standard deviations between calculated and observed pentad/heptad distributions were higher for the new assignments, but were certainly within a range of acceptability. The most significant *mrrr*-centered heptads are *mmrrrm* + *mmrrrr*, where a more substantial resonance intensity could be observed.

The fits between experimental pentad/heptad distributions and those calculated from the various two- and three-state models were accomplished with the Excel "solver" routine by minimizing the standard deviations between observed and calculated results. All the fits obtained in this study were from iterations that gave the lowest possible minimum in the standard deviation. The "solver" routine is iterative and more than one satisfactory solution is routinely possible, particularly for the fractions with high molar masses and low *racemic* contents, as will be discussed later. In Table 1, it can be seen that all of the models yielded calculated pentad/heptad distributions within experimental error of the observed distributions. The pentad/heptad experimental distribution in Table 1 is valid to three significant figures, as suggested by the fits, but the accuracy of the fourth significant figure is in doubt.

## Two and Three State Statistical Models

A description of *meso*/*racemic* sequence distributions in terms of Markovian transition probabilities has been given previously.[8−11] In this study, the nomenclature of Busico has been employed to designate each state in the two and three-state models.[2] Es is used for the enantiomorphic site control state, *C1* for the state that has two enantiomorphic sites where chain growth can occur at either site by "switching" back and forth, and CE for the chain-end control state. We use CE1 in this study to designate the use of first-order Markovian statistics in place of Bernoullian statistics in the so modified two- and three-state models. The following two- and three-state models were evaluated:

| | models | | |
|---|---|---|---|
| | no. parameters | type | refs |
| Es/CE | 3 | $P_0$ (or $\sigma$), $P_m$ and $X^a$ | 6, 7 |
| Es/CE1 | 4 | $P_0$, $P_{mr}$, $P_{rm}$, and $X$ | 3 |
| *C1*/CE | 6 | $^1P_0$, $^2P_0$, $P_{12}$,[b] $P_{21}$, $P_m$, and $X$ | 2 |
| *C1*/CE1 | 7 | $^1P_0$, $^2P_0$, $P_{12}$, $P_{21}$, $P_{mr}$, $P_{rm}$, and X | |
| Es/*C1*/CE | 8 | $P_0$, $^1P_0$, $^2P_0$, $P_{12}$, $P_{21}$, $P_m$, $X$, and $Y^c$ | 2 |
| Es/*C1*/CE1 | 9 | $P_0$, $^1P_0$, $^2P_0$, $P_{12}$, $P_{21}$, $P_{mr}$, $P_{rm}$, $X$, and $Y$ | |

[a] $X$ = fraction of chains produced by enantiomorphic site control. [b] 1 and 2 indicate sites 1 and 2 respectively. [c] $Y$ = fraction of chains produced by the CE state.

**Table 2. Transition Probabilities for Individual States for Various Statistical Models for Zf97K1.03**

| Es/CE | nc[a] | Es/CE1 | nc | *C1*/CE | nc | *C1*/CE1 | nc | Es/C1/CE | nc | $P_0 = 0.9995$ $^1P_0 = {}^2P_0$ | Es/*C1*/CE1 | nc | $P_0 = 0.9995$ $^1P_0 = {}^2P_0$ |
|---|---|---|---|---|---|---|---|---|---|---|---|---|---|
| $P_0$ | 0.9899 | $P_0$ | 0.9927 | $^1P_0$ | 0.9985 | $^1P_0$ | 0.9872 | $P_0$ | 0.9996 | 0.9995 | $P_0$ | 0.9995 | 0.9995 |
| $P_1$ | 0.0101 | $P_1$ | 0.0073 | $^1P_1$ | 0.0015 | $^1P_1$ | 0.0128 | $P_1$ | 0.0004 | 0.0005 | $P_1$ | 0.0005 | 0.0005 |
| $P_m$ | 0.2267 | $P_{mr}$ | 0.1914 | $^2P_0$ | 0.8839 | $^2P_0$ | 1.0000 | $^1P_0$ | 0.9308 | 0.9277 | $^1P_0$ | 0.9237 | 0.9225 |
| $P_r$ | 0.7733 | $P_{mm}$ | 0.8086 | $^2P_1$ | 0.1161 | $^2P_1$ | 0.0000 | $^1P_1$ | 0.0692 | 0.0723 | $^1P_1$ | 0.0763 | 0.0775 |
| [Es] | 0.9843 | $P_{rm}$ | 0.2869 | $P_{12}$ | 0.0674 | $P_{12}$ | 0.0744 | $^2P_0$ | 0.9005 | 0.9277 | $^2P_0$ | 0.9066 | 0.9225 |
| [CE] | 0.0157 | $P_{rr}$ | 0.7131 | $P_{11}$ | 0.9326 | $P_{11}$ | 0.9256 | $^2P_1$ | 0.0995 | 0.0723 | $^2P_1$ | 0.0934 | 0.0775 |
| std dev | 0.00109 | [Es] | 0.9562 | $P_{21}$ | 0.9186 | P21 | 0.2239 | $P_{12}$ | 0.0999 | x | $P_{12}$ | 0.0500 | x |
| | | [CE1] | 0.0438 | $P_{22}$ | 0.0814 | $P_{22}$ | 0.7761 | $P_{11}$ | 0.9001 | x | $P_{11}$ | 0.9500 | x |
| | | std dev | 0.00068 | $P_m$ | 0.2269 | $P_{mr}$ | 0.1914 | $P_{21}$ | 0.8501 | x | $P_{21}$ | 0.9000 | x |
| | | | | $P_r$ | 0.7731 | $P_{mm}$ | 0.8086 | $P_{22}$ | 0.1499 | x | $P_{22}$ | 0.1000 | x |
| | | | | [*C1*] | 0.9843 | $P_{rm}$ | 0.2868 | $P_m$ | 0.1083 | 0.1115 | $P_{mr}$ | 0.0074 | 0.0073 |
| | | | | [CE] | 0.0157 | $P_{rr}$ | 0.7132 | $P_r$ | 0.8917 | 0.8885 | $P_{mm}$ | 0.9926 | 0.9927 |
| | | | | std dev | 0.00109 | [*C1*] | 0.9563 | [Es] | 0.1761 | 0.1756 | $P_{rm}$ | 0.2161 | 0.2161 |
| | | | | | | [CE1] | 0.0437 | [*C1*] | 0.8167 | 0.8171 | $P_{rr}$ | 0.7839 | 0.7839 |
| | | | | | | std dev | 0.00068 | [CE] | 0.0072 | 0.0073 | [Es] | 0.1331 | 0.1334 |
| | | | | | | | | std dev | 0.00084 | 0.00084 | [*C1*] | 0.5170 | 0.5138 |
| | | | | | | | | | | | [CE1] | 0.3499 | 0.3528 |
| | | | | | | | | | | | std dev | 0.00083 | 0.00083 |

[a] Key: nc = no constraints.

Definitions of the above parameters have been given previously by Busico[2]. It should be recalled that the following pairs of transition probabilities sum to unity: $P_0 + P_1$, $P_m + P_r$, $P_{mm} + P_{mr}$, $P_{rr} + P_{rm}$, $P_{11} + P_{12}$ and $P_{22} + P_{21}$. As mentioned earlier, it seemed appropriate to test the Chûjô/Doi and Busico two- and three-state statistical fits after changing the CE state from zero to first-order Markovian statistics.[3,20]

In Table 1, it can be seen that satisfactory fits were obtained with all of the above models. The fits for Es/CE vs *C1*/CE and the corresponding models, Es/CE1 vs *C1*/CE1, are identical. It will be seen from equations introduced later that the *C1*/CE and *C1*/CE1 models reduce to Es/CE and Es/CE1, respectively, whenever there is a $^1P_0$, $^2P_0$ equality or $P_{11} = P_{21} =$ unity. The closeness of $^1P_0$ and $^2P_0$ in the two models containing a *C1* state can be seen in Table 2. The invariance of the partitioning parameters, that is, [Es],[CE] vs [*C1*],[CE] and also [Es],[CE1] vs [*C1*],[CE1], as seen in Table 2, is another indicator of a *C1* state that is behaving as an Es state.

Fitting the three-state models is more difficult because there is a high number of parameters as well as low signal/noise ratios for the weaker resonances, which are now more important. As observed for the two-state models, the *C1* states in the two three-state models are also converging toward an Es state. As the value for $^1P_0$ approaches $^2P_0$ in the *C1* state for any model containing this component, the values for the "switching" parameters, $P_{11}$, $P_{12}$, $P_{21}$, and $P_{22}$, become less relevant. Under such circumstances, a second Es state, as opposed to a *C1* state, appears to be more feasible in a three-state analysis of a highly isotactic poly(propylene).

In an earlier Es/*C1*/CE study by Busico et al.[2], a *C1* state, which was devoid of any Es character, was required to fit sequence distribution data from a lowly isotactic poly(propylene). In the present study on a highly isotactic poly(propylene), we chose to test the Es/*C1*/CE1 model with a *C1* state, instead of a second Es state, to establish if we could distinguish a perfect Es state from a *C1* state that had small, but possibly real differences in $^1P_0$ and $^2P_0$. The flexibility of a *C1* state is appealing because it will move in the direction of a second Es state if dictated by the data, as demonstrated by the behavior of the corresponding two-state models. As it turns out, the pentad/heptad data in Table 1 did not permit us to distinguish between a pure Es state and a *C1* state with small differences in $^1P_0$ and $^2P_0$, because both fits were within experimental error of the observed pentad/heptad distribution. See Tables 2 and 3 where transition probabilities from analyses without constraints are compared to those with $^1P_0 = {}^2P_0$.

What is most pertinent in the present three-state model fits is the partitioning among the various states because information is obtained about the polypropylene composition distribution. The results from the various models will later be examined for consistencies with the fractionation and crystallization behavior.

The Excel solver routine fits for Es/*C1*/CE and Es/*C1*/CE1 had strong tendencies to give minima with $P_0$ for the Es component equal to unity. This result leads to the conclusion that the Es state in both the Es/*C1*/CE and Es/*C1*/CE1 three-state models is extremely isotactic with very few stereodefects. A similar observation was made by Busico with his three-state, Es/*C1*/CE model on sequence data from a much lesser isotactic polypropylene.[2] The fact that the present data also led to a $P_0$ of unity affords an opportunity to eliminate this parameter from the iteration process by setting it equal to unity or 0.9995. Even though a $P_0$ of unity is not a truly realistic possibility under most circumstances, the precision of the data would not distinguish, for example, a $P_0$ of 0.9995 from 1.0000.

Other equalities, $^1P_0 = {}^2P_0$ and $P_{11} = P_{21} = 1$ were also imposed during the three-state model iteration processes to evaluate the value of having a second, pure Es state as opposed to a *C1* state. Once again, an introduction of these equalities mathematically forces the *C1* state to become a second Es state in the three-state model. In all cases, a final iteration, where all parameters were allowed to float, was performed. Complete results for Zf97K1.03 are given in Table 2. Corresponding data from the fractions are given in Table 3. The closeness of the values for $^1P_0$ and $^2P_0$ in the fits with no constraints indicated that the *C1* component in the three state models had reduced within experimental error to a second Es state. In each case, the same standard deviations and similar pentad/heptad distribution fits were obtained with and without the constraints. What was most important was that the partitioning among the three states was invariant to differences in the "switching" parameters in the *C1*

**Table 3. Summary of Results from the Es/*C1*/CE1 Three-State Model for All Fractions**

| | | fraction | | | | | | | | | |
|---|---|---|---|---|---|---|---|---|---|---|---|
| | | parent Z263K0.51 | | Zf97K1.03 | | Zf163K0.60 | | Zf204K0.41 | | Zf328K0.36 | |
| | | nc[a] | $P_0 = 0.9995$ $^1P_0 = {}^2P_0$ | nc | $P_0 = 0.9995$ $^1P_0 = {}^2P_0$ | nc | $P_0 = 0.9995$ $^1P_0 = {}^2P_0$ | nc | $P_0 = 0.9995$ $^1P_0 = {}^2P_0$ | nc | $P_0 = 0.9995$ $^1P_0 = {}^2P_0$ |
| Es | $P_0$ | 0.9941 | 0.9995 | 0.9995 | 0.9995 | 0.9995 | 0.9995 | 0.9966 | 0.9995 | 0.9988 | 0.9995 |
| | $P_1$ | 0.0059 | 0.0005 | 0.0005 | 0.0005 | 0.0005 | 0.0005 | 0.0034 | 0.0005 | 0.0012 | 0.0005 |
| *C1*-1 | $^1P_0$ | 0.7647 | 0.8624 | 0.9237 | 0.9225 | 0.9616 | 0.9524 | 0.8649 | 0.9140 | 0.9073 | 0.9181 |
| | $^1P_1$ | 0.2353 | 0.1376 | 0.0763 | 0.0775 | 0.0384 | 0.0476 | 0.1351 | 0.0860 | 0.0927 | 0.0819 |
| *C1*-2 | $^2P_0$ | 0.7419 | 0.8624 | 0.9066 | 0.9225 | 0.9001 | 0.9524 | 0.8718 | 0.9140 | 0.8443 | 0.9181 |
| | $^2P_1$ | 0.2581 | 0.1376 | 0.0934 | 0.0775 | 0.0999 | 0.0476 | 0.1282 | 0.0860 | 0.1557 | 0.0819 |
| | $P_{12}$ | 0.2010 | x | 0.0500 | x | 0.1000 | x | 0.1001 | x | 0.1011 | x |
| | $P_{11}$ | 0.7990 | x | 0.9500 | x | 0.9000 | x | 0.8999 | x | 0.8989 | x |
| | P21 | 0.6666 | x | 0.9000 | x | 0.7999 | x | 0.8499 | x | 0.9487 | x |
| | P22 | 0.3334 | x | 0.1000 | x | 0.2001 | x | 0.1501 | x | 0.0513 | x |
| CE1 | $P_{mr}$ | 0.0002 | 0.0002 | 0.0074 | 0.0073 | 0.0036 | 0.0036 | 0.0004 | 0.0003 | 0.0011 | 0.0011 |
| | $P_{rm}$ | 0.0577 | 0.0387 | 0.2161 | 0.2161 | 0.3756 | 0.3752 | 0.1340 | 0.1043 | 0.1303 | 0.1259 |
| | [C1] | 0.0272 | 0.0650 | 0.1331 | 0.1334 | 0.1027 | 0.1027 | 0.0253 | 0.0569 | 0.0315 | 0.0434 |
| | [Es] | 0.5200 | 0.6577 | 0.5170 | 0.5138 | 0.4935 | 0.4944 | 0.5119 | 0.5149 | 0.7036 | 0.7039 |
| | [CE1] | 0.4528 | 0.2773 | 0.3499 | 0.3528 | 0.4038 | 0.4029 | 0.4628 | 0.4283 | 0.2650 | 0.2527 |
| | std dev | 0.00074 | 0.00075 | 0.00083 | 0.00083 | 0.00059 | 0.00059 | 0.00032 | 0.00032 | 0.00040 | 0.00040 |

[a] Key: nc = no constraints.

state. The data did not allow us to distinguish between a perfect Es state and a *C1* state that was close, but not a perfect Es state. For those fractions where a $P_0$ of unity was obtained, a constraint of 0.9995 was introduced when determining values for the remaining parameters. See the parameters for the three-state models in Table 2. The important state fractions and the Es and CE1 parameter values are not significantly affected by the choice of either a *C1* or Es state in the three-state model in this application on a highly isotactic poly(propylene).

The standard deviations for all of the fits for Es/*C1*/CE1 varied from 0.0003 to 0.0008. They are better than should be expected considering that the experimental error could be as high as 50−100% for the very weak pentads and heptads in the 0.0003 to 0.0010 range. The use of nine required variables for a pure Es/*C1*/CE1 model does not help matters in establishing fits because any time the number of variables is increased for only 14 independent observations, a more conforming fit is likely. This is why reducing the number of parameters, whenever indicated, is important. For the individual fraction analyses utilizing the Es/*C1*/CE1 three-state model, $P_0$ was set to 0.9995 and $^1P_0$ was set equal to $^2P_0$, as indicated by the results from the overall iterative fits. This converts Es/*C1*/CE1 to an $Es_1/Es_2$/CE1 three-state model. See Table 3. This modification reduces the number of parameters in the iterative fits from nine to six with 14 independent observations. Another important factor in the statistical analyses was the capability of performing the iterative fits over a series of fractions from the same sample. Independent Excel "solver" solutions that show anticipated trends as the fractions increased in molar mass should add validity to the fits. The complexity of either three-state model would lower confidence in the results obtained from only a single analysis.

One significant observation that persisted among all of the fits for Es/*C1*/CE1 three-state model is that $P_{mr}$ is exceedingly small and only ranges from 0.0003 to 0.0073 among the various fractions. See Table 3. This result leads to a high $P_{mm}$ and the long isotactic sequence lengths obtained for the CE1 component. This result only occurred after the use of first-order Markovian statistics for the chain-end control component in a three-state model that also contained a *C1* or second Es state.

## Sequence Length Distributions

Statistical fits are typically evaluated from the magnitudes of the standard deviations between experimental and calculated pentad/heptad distributions. Triad distributions, diad distributions, average *meso* sequence lengths, average *meso* run lengths (MRL), and standard deviations are given with the calculated vs observed pentad/heptad observed distributions in Table 1 for the Zf97K1.03 fraction. The transition probabilities determined from each of the models are given in Table 2. Excellent fits were also achieved with the other fractions and the analytical trends that occur with increasing fraction molar mass will be discussed later.

In Table 1, the pentad/heptad distributions predicted from all of the two- and three-state model analyses are found to be strikingly similar and to fall well within experimental error of the measurements. Corresponding observations were made for the other fractions. On the basis of the similarities of the pentad/heptad distributions predicted by the various models, there is no discriminating basis to choose any particular model. At this point, it was necessary to find some other criteria that could possibly distinguish the various model behaviors.

In contrast to the observed consistency of the variously calculated pentad/heptad distributions, sequence distribution curves, calculated with the same individual state transition probabilities, were found to show distinct and identifying differences for the various models. In particular, they were extremely useful when trying to establish how appropriate each model might be in light of the crystallization and fractionation data.

Sequence distribution curves can be calculated in more than one manner. One approach is a simple plot of $[r(m)_i r]$ vs sequence length, "*i*", and another is $i[r(m)_i r]$ vs "*i*" for $i = 1$ to $i = n$. The former is a plot of the sequence fraction vs "*i*" while the latter is a plot of the *meso* diad fraction at sequence length "*i*" vs "*i*". Sequence fraction vs sequence length plots give simple decaying exponential types of curves because the highest term numerically is [*rmr*], followed by [*rmmr*], [*rmmmr*], etc. Plots of the sequence *meso* diad fractions

vs "i" are more useful and give the results shown in Figures 1−3. For these calculated sequence distribution curves, "i" was varied in increments from 1 to 5000. The *meso* diad fractions at each sequence length, are defined below:

| | |
|---|---|
| $i = 1$ | $[m]_1 = [rmr]$ |
| $i = 2$ | $[m]_2 = 2[rmmr]$ |
| $i = 3$ | $[m]_3 = 3[rmmmr]$ |
| • | • |
| • | • |
| • | • |
| $i = n$ | $[m]_n = n[r(m)_n r]$ |

Summing the individual diad fractions from $i = 1$ to $n$ gives the overall *meso* diad fraction, $[m]$. Substituting $P_0$ in the asymmetric chain component, Es, expression for $[m]_i$ gives in the Es/CE model, for example

$$([m]_i)_{\mathrm{Es}} = i[X]\{[1]^2[0]^{i+1} + [0]^2[1]^{i+1}\} = i[X]\{[1 - P_0]^2[P_0]^{i+1} + [P_0]^2[1 - P_0]^{i+1}\} \quad (1)$$

for sequence length, "*i*". Likewise, $[m]_i$, in terms of the symmetric chain component (CE) is

$$([m]_i)_{\mathrm{CE}} = i[1 - X][1 - P_m]^2[P_m]^i \quad (2)$$

Multiplying the above expressions for the asymmetric and symmetric chain *meso* diad fractions at each sequence length by $[X]$ and $[1 - X]$, respectively, for the Es/CE model yields plots where the areas under the sequence distribution curves are related to the amount present.

For the *C1* switching state, which is analogous to that proposed by Cossee,[25]

$$[0] = 0.5({P_{11}}^1P_0 + {P_{21}}^1P_0 + {P_{22}}^2P_0 + {P_{12}}^2P_0) \quad (3)$$

and

$$[1] = 0.5[P_{11}(1 - {}^1P_0) + P_{21}(1 - {}^1P_0) + P_{22}(1 - {}^2P_0) + P_{12}(1 - {}^2P_0)] \quad (4)$$

These expressions are used to determine $[m]_i$ for the *C1* state in the Es/*C1*/CE three-state models, for example, as follows:

$$([m]_i)_{\mathrm{C1}} = i[1 - X - Y]([1]^2[0]^{i+1} + [0]^2[1]^{i+1}) \quad (5)$$

Here "*X*" and "*Y*" are the fractions of the Es and CE components, respectively, for the Es/*C1*/CE model and [0] and [1] are defined by eqs 3 and 4, respectively.

Equations 3 and 4 reduce to the Es case by substituting ${}^1P_0 = {}^2P_0$. The *C1* state will also reduce to the alternating mechanism through which monomer insertions occur with a metallocene catalyst[26] whenever $P_{12} = P_{21} = 1$. Thus, eqs 3 and 4 are consistent with using an Es state in configurational pentad/heptad analyses of poly(propylene)s produced with a metallocene catalyst.[15] Finally, $([m]_i)_{\mathrm{CE1}}$ is given by

$$([m]_i)_{\mathrm{CE1}} = i[\mathrm{Y}][P_{mr}P_{rm}[P_{mm}]^{(i-1)}P_{mr}/(P_{rm} + P_{mr}) \quad (6)$$

Equation 6 can be used in the appropriate two and three-state models after making a proper substitution for "*Y*". Values for the transition probabilities, obtained from the pentad/heptad sequence distribution fits with each model, were substituted into each of the above equations for $[m]_i$ to give the various state sequence length distributions.

Other equations utilized to evaluate the quality of the various fits are given below

$$\text{average } meso \text{ sequence length} = \bar{n}_m = \sum_i i[r(m)_i r]/\sum_i [r(m)_i r] = 2[m]/[mr + rm] \quad (7)$$

where the sums are over $i = 1$ to $i = n$ and

$$\text{average } meso \text{ run length} = \mathrm{MRL} = 2[mmmm]/[mmmr + rmmm] \quad (8)$$

Plots of $[m]_i$ vs $i$ show differences for the poly(propylene) molecules arising from each state in the two- and three-state models as shown in parts a−c of Figure 1, where composite curves are plotted for all six of the statistical models for the Zf97K1.03 fraction. In Figure 1a for the Es/CE model, it can be seen that the CE component is a predominantly syndiotactic poly(propylene) because the sequence distribution curve peaks at $i = 1$ and falls to a *meso* diad fraction of $10^{-5}$ at $i = 5$. The Es component peaks around $i = 100$ and falls to an $[m]_i$ of $10^{-5}$ at $i = 900$. The Es/CE model therefore predicts the presence of a mostly syndiotactic poly(propylene) mixed with a predominantly isotactic poly(propylene).

Modification of the Es/CE state model with a first-order Markovian symmetric chain component (CE1) extends the peaks of the sequence distribution curves for both the Es and CE1 components, as is also shown in Figure 1a. CE1, which is now much lesser syndiotactic than the CE component in Es/CE, peaks at $i = 5$ and reaches an $[m]_i$ of $10^{-5}$ near $i = 35$. The Es component of Es/CE1, which is now somewhat more isotactic than the Es component in Es/CE, peaks at $i = 150$ and reaches an $[m]_i$ of $10^{-5}$ close to $i = 1200$. This trend was observed uniformly in all of the models for all of the fractions whenever CE was changed to CE1.

Sequence distribution curves for Zf97K1.03 for the *C1*/CE model and that modified by changing CE to CE1 are given in Figure 1b. As anticipated from the respective sets of transition probabilities, the curves for *C1*/CE vs Es/CE and *C1*/CE1 vs Es/CE1 are nearly the same. As discussed previously, the circumstances are present that causes *C1* to reduce essentially to an Es state. An important observation is that the flexibility of the *C1* state allowed a *C1* → Es result after an insertion of data.

A different result was obtained with the Es/*C1*/CE model. The transition probabilities from the model analyses are given in Table 2 and the sequence distribution curves are shown in Figure 1c. In the Es/*C1*/CE model for the Zf97K1.03 fraction, the sequence distribution curve for the CE component peaks at $i = 1$ and falls to a *meso* diad fraction of $10^{-5}$ at $i = 4$. The *C1* component peaks at $i = 10$ and falls to an $[m]_i$ of $10^{-5}$ at $i = 100$. The Es component is extremely isotactic as a consequence of obtaining a $P_0$ of unity. The constraints of 0.9995 for $P_0$ and ${}^1P_0 = {}^2P_0$ were used in the plot in Figure 1c. In contrast, the *C1* component (or second Es component) is only weakly isotactic. It is surprising that a predominantly syndiotactic poly(propylene) is still predicted for the CE component. Attempts to avoid this result by starting the iterative process with higher values of $P_m$ were unsuccessful.

By far, the most different sequence distribution curves were obtained with Es/*C1*/CE1. The CE1 component

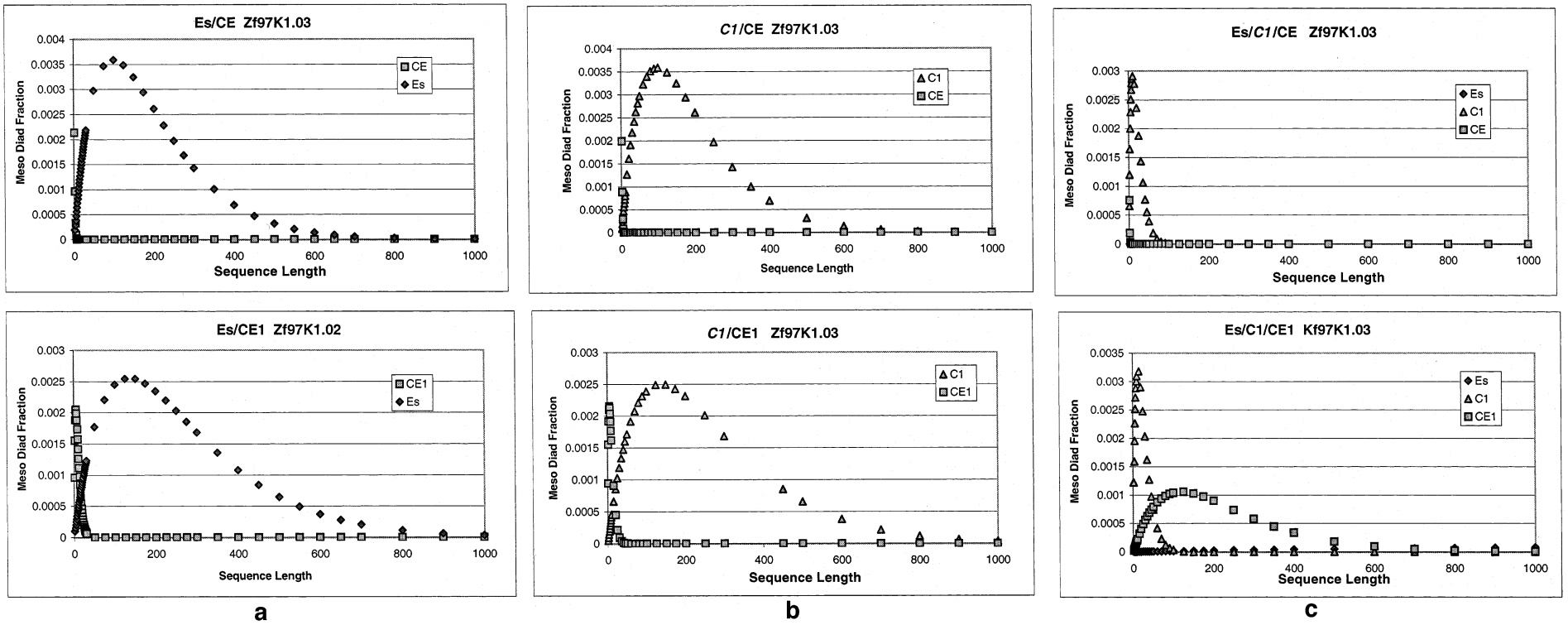


**Figure 1.** (a) Sequence lengths vs *meso* diad fractions for two-state models, Es/CE and Es/CE1. (b) Sequence lengths vs *meso* diad fractions for two-state models, *C1*/CE and *C1*/CE1. (c) Sequence lengths vs *meso* diad fractions for three-state models, Es/*C1*/CE and Es/*C1*/CE1.

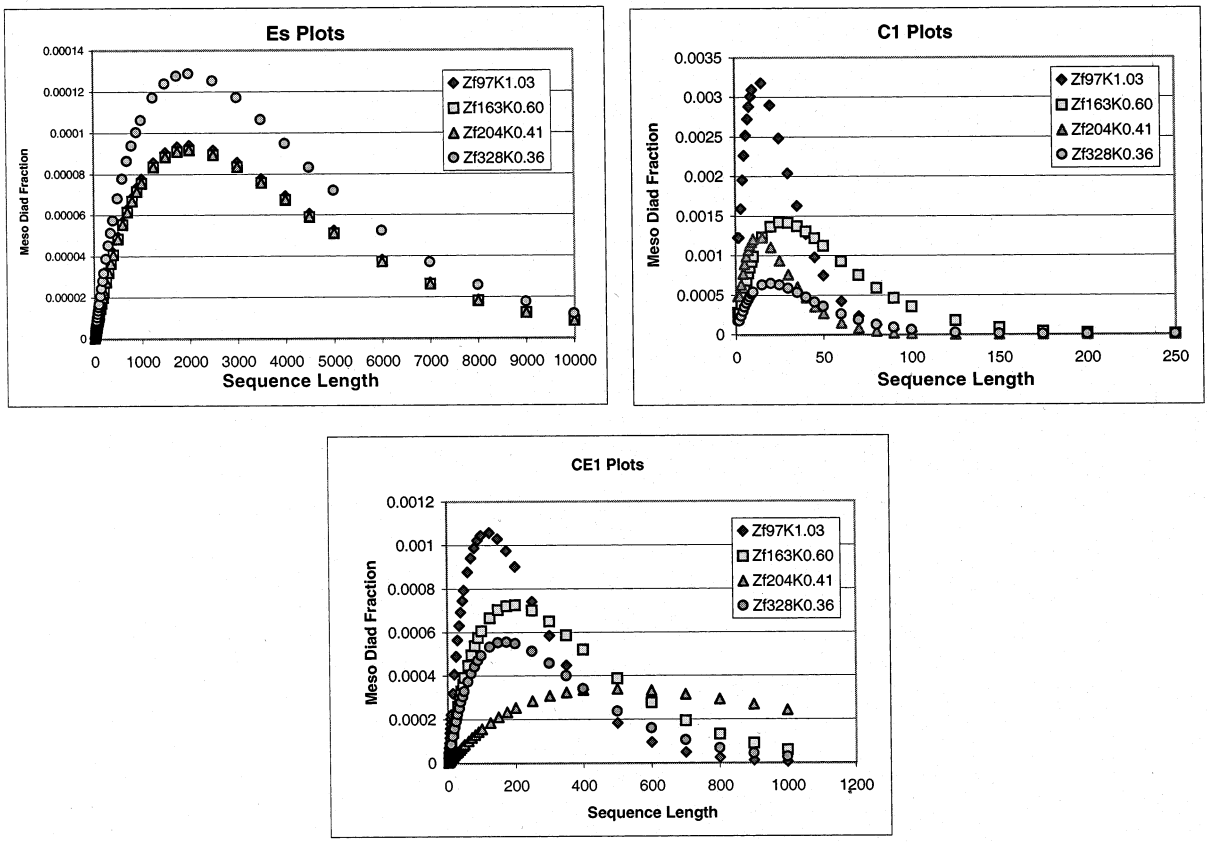


**Figure 2.** Es/*C1*/CE1 three-state model: plots of individual fractions for *C1* and CE1.

now peaks at $i = 250$ and $[m]_i$ reaches $10^{-5}$ at $i = 1000$. The *C1* (or second Es) component peaks at $i = 15$ and $[m]_i$ reaches $10^{-5}$ by $i = 100$. The primary Es component is extremely isotactic as a consequence of, once again, obtaining unity for $P_0$. The Es/*C1*/CE1 model predicts the presence of an almost defect free, highly isotactic poly(propylene) component, a mainly isotactic poly(propylene) component that has short, blocky syndiotactic defects and a weakly isotactic, stereoblock component. A predominantly syndiotactic poly(propylene) component, significantly, is not predicted.

## Results and Discussion

It was established from the $^{13}C$ NMR characterization of the four fractions that the stereodefect concentrations decrease (or the average isotactic sequence lengths increase) with increasing molar mass.[14] As discussed previously, the Es/*C1*/CE1 model analyses permits each fraction to be broken down into three different types of isotactic poly(propylene) molecules by microstructure. It is important to establish the trends that occur among the sequence distributions for each fraction as the molar mass increases. This particular three-state model is the only one that gives two different types of highly isotactic chains in accord with TREF results.[4] The number of parameters was reduced by setting $P_0 = 0.9995$ and $^1P_0 = {}^2P_0$, as indicated by the results when these parameters were allowed to float. Consistent sets of transition probabilities were obtained for the various fractions as can be seen in Table 3 for the parent poly(propylene) and its fractions. This consistency will lead to sequence distribution curves that will be correspondingly similar for each of the fractions. In Figure 2, the sequence distribution behaviors for the Es, *C1*, and CE1 components in each fraction are monitored independently as the sequence lengths increase, as shown by separate composite plots. With a value for $P_0$ set at 0.9995, the peaks of the Es curves will be the same. As anticipated from the values of the observed transition probabilities, none of the component microstructures in each fraction show any significant changes with increasing molar mass. The CE1 sequence distribution curves from the three-state models peak between $i = 125$ and 200 for three of the four fractions. Only Zf204K0.41, which peaks near $i = 500$ differs from that of the other components. The *C1* component sequence distribution curves peak at around 15, once again for three of the four fractions. The only exception is a peak at a slightly longer sequence length for the Zf163K0.61 fraction. The same states for each fraction show similar peaks in the fraction sequence distribution curves despite differences in the fraction molar masses and overall *racemic* contents.

**Table 4. Calculated Racemic Contents for Each of the Components in the Es/*C1*/CE1 Model**

| | [*racemic*] | | |
|---|---|---|---|
| fraction | Es | CE1 | *C1* |
| Zf97K1.03 | 0.001 | 0.03 | 0.14 |
| Zf163K0.60 | 0.001 | 0.01 | 0.09 |
| Zf204K0.41 | 0.001 | 0.01 | 0.14 |
| Zf328K0.36 | 0.001 | 0.01 | 0.15 |

The amounts of the *C1* component decrease substantially with increasing molar mass, as can be seen in Table 3. The Es content is the highest in the Zf328K0.36 fraction while the relative amounts of CE1 only change nominally with successive fractions. This behavior causes the weighted average for the *racemic* contents over the three components in the series of fractions to decrease with increasing molar mass. Table 4 lists the

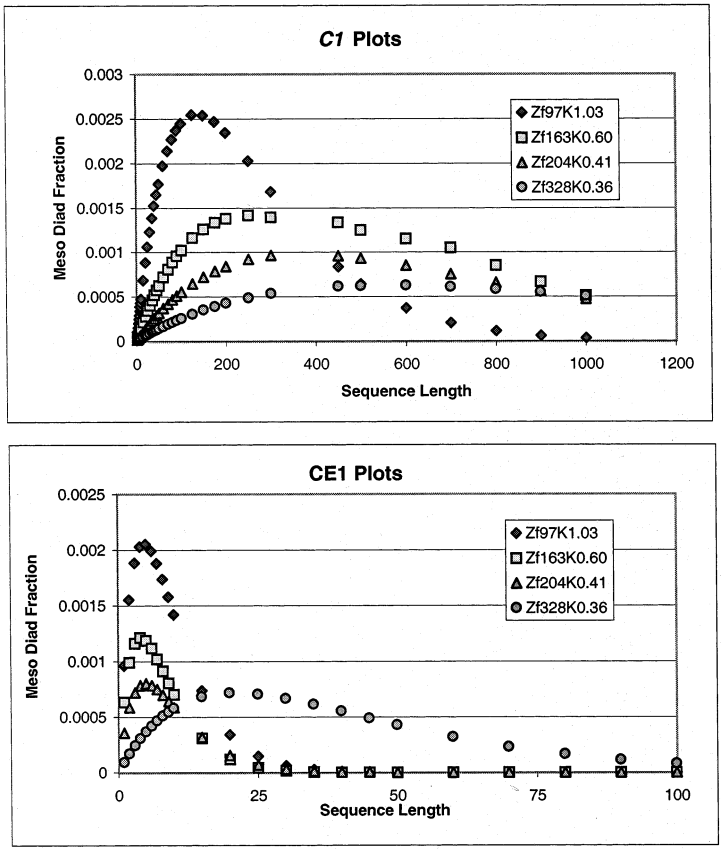


**Figure 3.** *C1*/CE1 two-state model: plots of individual fractions for *C1* and CE1.

calculated *racemic* contents independently for Es, *C1*, and CE1 states for each fraction where it can be seen there is a consistency among *racemic* contents for each respective state. The calculated *racemic* contents for each state increase by approximately an order of magnitude, respectively, when going from Es to CE1 to *C1*. This model result, which differs from that of the other two- and three-state models, leads to the conclusion that the microstructures of the three types of Ziegler−Natta poly(propylene)s are similar in each fraction and it is primarily the component amounts and molecular weights that change with successive fractions. Thus, the behavior of the individual states in the Es/*C1*/CE1 model results for the various fractions indicate narrow composition distributions similar to that observed for the single-sited metallocene catalyst.[14] It is only the changes in the distributions of the components that account for the decreasing *racemic* content with increasing molar mass.

The relative differences in molecular weights of the components in the various two- and three-state models can be inferred from their respective *racemic* contents. The observed trend of a decreasing *racemic* content with increasing molar mass in this study follows the suggestion by Chadwick,[27] who proposed that chain transfer reactions are increased by the presence of dormant chains, which, in part, are related to the *racemic* content. The Es component, with the lowest *racemic* content, is expected to have the highest molar mass, followed by the CE1 component and finally the *C1* component, which has the highest *racemic* content and is expected to have the lowest molar mass. Chadwick suggested that chains ending in syndiotactic and 2,1-regiodefects give higher levels of chain transfer with hydrogen than do growing chains ending with a *meso* diad.[27] Thus, the states with the higher *racemic* contents are expected to have the lower molar masses. Accordingly, the CE1 and *C1* states are expected to decrease in amounts relative to the Es component with increasing molar mass of the fractions. A decreasing [*r*] with molar mass has been independently reported in TREF studies of $MgCl_2$ supported Ziegler−Natta poly(propylene)s by Morini et al.[4] It would appear that the molecular weight distributions of both the CE1 and *C1* components have sufficient breadths to give decreasing amounts in each successive fraction as the molar masses increase. Thus, it is the way that the three types of components combine at each molar mass that is responsible for the frequent observation that the stereodefect concentrations decrease with increasing molar mass.[5,14,27] As will be seen in the later discussion of the fraction crystallization behavior, it is important for a model to predict individual component microstructures that are reasonably invariant to increasing molar mass.

For comparison purposes, Figure 3 contains similar composite plots for the *C1*/CE1 two-state model, which is representative of the results from the other two-state models. From the sequence distribution curves shown in Figures 2 and 3, it is easily ascertained that the *C1*/CE1 two-state model and the Es/*C1*/CE1 three-state model lead to quite different predictions for the sequence distribution curves for the four fractions. The predicted pentad/heptad distributions, triad and diad distributions and average sequence lengths for the *meso* runs for these two models are all within experimental error of the corresponding observed results, as can be seen in Table 1. In contrast to the pentad/heptad behaviors, the *C1*/CE1 two-state model has *C1* sequence distributions curves that peak at $i = 100$ for the Zf97K1.03 fraction, at $i = 250$ for the Zf163K0.60 fraction, at $i =$

**Table 5. Calculated Pentad/Heptad Distributions for Each Component in *C1*/CE1, Es/*C1*/CE1 Models for Zf97K1.03**

| pentad/ heptad | *C1*/CE1 model | | Es/*C1*/CE1 model | | |
|---|---|---|---|---|---|
| | C1 | CE1 | Es | C1 | CE1 |
| *mmmm* | 0.9639 | 0.3172 | 0.9974 | 0.6680 | 0.9479 |
| *mmmr* | 0.0142 | 0.1501 | 0.0010 | 0.1124 | 0.0135 |
| *rmmr* | 0.0001 | 0.0178 | 0.0000 | 0.0051 | 0.0000 |
| *mmrr* | 0.0142 | 0.1324 | 0.0010 | 0.1124 | 0.0107 |
| *mmrm* | 0.0001 | 0.0532 | 0.0000 | 0.0102 | 0.0029 |
| *rrmr* | 0.0001 | 0.0313 | 0.0000 | 0.0102 | 0.0001 |
| *rmrm* | 0.0001 | 0.0126 | 0.0000 | 0.0102 | 0.0000 |
| *mrrrrm* | 0.0001 | 0.0119 | 0.0000 | 0.0040 | 0.0007 |
| *mrrrrr* | 0.0000 | 0.0594 | 0.0000 | 0.0007 | 0.0052 |
| *rrrrrr* | 0.0000 | 0.0739 | 0.0000 | 0.0004 | 0.0094 |
| *rmrrrm* | 0.0000 | 0.0064 | 0.0000 | 0.0007 | 0.0000 |
| *rrrrmr* | 0.0000 | 0.0159 | 0.0000 | 0.0007 | 0.0001 |
| *mmrrrm* | 0.0000 | 0.0271 | 0.0000 | 0.0007 | 0.0018 |
| *mmrrrr* | 0.0001 | 0.0673 | 0.0000 | 0.0080 | 0.0066 |
| *rmrrmr* | 0.0000 | 0.0009 | 0.0000 | 0.0004 | 0.0000 |
| *rmrrmm* | 0.0001 | 0.0073 | 0.0000 | 0.0080 | 0.0000 |
| *mmrrmm* | 0.0070 | 0.0153 | 0.0005 | 0.0478 | 0.0011 |
| sum | 1 | 1 | 1 | 1 | 1 |
| [*m*] | 0.9854 | 0.5998 | 0.9990 | 0.8570 | 0.9683 |
| [*r*] | 0.0146 | 0.4002 | 0.0010 | 0.1430 | 0.0317 |

450 for the Zf204K0.41 fraction, and at $i = 600$ for the Zf328K0.36 fraction. The CE1 sequence distribution curves peak at $i = 1$ for the Zf97K1.03 fraction, at $i = 20$ for the Zf163K0.60 fraction, at $i = 5$ for the Zf204K0.41 fraction, and at $i = 25$ for the Zf328K0.36 fraction. It will be discussed later that this model is not consistent with the crystallization data. As discussed previously, the CE1 component is now a weakly isotactic poly(propylene) with runs of syndiotactic sequences disrupting the isotactic blocks. This behavior, which is similar to that of the various two-state models, is quite different from that predicted with the Es/*C1*/CE1 three-state model.

A successful model will also be consistent with the observed trends in the fractionation data as well as with the results from the fraction crystallization studies. One result that is difficult to accept from the predictions of any of the two-state models is the unlikely possibility that any syndiotactic or lowly isotactic component would survive for very long during the fractionation. It is reasonable to find substantially lesser isotactic chains in the lower molar mass fractions but it is difficult to propose that these components would still be present to any significant extent in the high molar mass fractions. Once again, the molar masses of any poly(propylene) are expected to be related to the *racemic* content, which leads to chain transfer and to the typically low molar masses observed for atactic poly(propylene)s.[27] Neither an atactic poly(propylene) nor a stereoblock isotactic poly(propylene) has been observed to exhibit a molar mass as large as that observed for a highly isotactic poly(propylene).[4,27]

It is also important from a mechanistic viewpoint[2] to establish which state in the Es/*C1*/CE1 three-state model gives rise to the blocky syndiotactic defects connecting much longer isotactic blocks. The *C1*/CE1 and Es/*C1*/CE1 models were broken down into predicted pentad/heptad distributions independently for the *C1*, CE1 and Es components. This can be accomplished with the transition probabilities derived from the model fits. Table 5 has complete sets of predicted pentad/heptad distributions for each state in the *C1*/CE1 and the Es/*C1*/CE1 models for Zf97K1.03. The Es state in the Es/*C1*/CE1 three-state model has no syndiotactic sequences other than those associated with defects having single inversions of configuration, which is the only type of stereodefect predicted for the Es state. The syndiotactic heptad sequences, observed in the overall pentad/heptad distribution, are predicted primarily by the CE1 state with only a small contribution from the *C1* switching (or Es) state in the Es/*C1*/CE1 model. The three states are predicted to be highly isotactic, stereoblock and mainly isotactic by the Es/*C1*/CE1 model, respectively, in accord with TREF results.[4] The prediction of an observable quantity of *mmrrrm* indicates the presence of isotactic blocks of opposite handedness for the mainly isotactic CE1 component. This result is consistent with the observed behavior that short syndiotactic connecting sequences are still found in the high molar mass fractions in this study and also with high concentrations of donor, which leads to high isotactic contents, as observed in earlier studies.[3,4]

The *C1* (or Es) state in the *C1*/CE1 two-state model is responsible for the predominantly isotactic component as seen in Table 5. Defects other than the 0001000 defect are predicted for this state, but the *rrrrrr* heptad is not predicted to arise from this component. The observed *rrrrrr* heptad sequences are predicted to arise only from the CE1 component, which, for this two-state model, is only weakly isotactic, ([*m*] = 0.6). Thus, the *rrrrrr* heptad would not be predicted to persist in the higher molecular weight fractions with lower defect concentrations. The prediction of short blocks of syndiotactic sequences connecting very long blocks of isotactic sequences by the Es/*C1*/CE1 model is an important result that is consistent with the fractionation and crystallization data. The importance of having a CE1 state in addition to a *C1* or second Es state in a three-state model to achieve this result cannot be overemphasized.

Finally, it is instructive to examine the predicted microstructures from the two- and three-state models for consistency with the observed crystallization behavior. For this purpose, focus is given to the observed invariance of the spherulitic linear growth rates of ZN fractions that have different levels of stereodefects. The data were presented in Figure 3B of the previous paper,[14] where it was also concluded that the overall crystallization rates would not correlate with the average defect microstructures of the poly(propylene) fractions. The overall crystallization rates are subject to differences in primary nucleation, possibly due to factors unrelated to chain microstructure. The invariance of the linear growth rates requires a microstructural model that comprises similar types of crystallizable sequences in all of the chains. A simplified scheme consistent with these data is shown in Figure 4B of the previous paper. It was proposed that a microstructural model with nonuniform intermolecular levels of stereodefects and a blocky intramolecular distribution of defects met the requirements for the observed fractionation data and the consistency of the linear growth rate data. The fact that none of the fractions, even the ones with the most defects, led to any significant content of the $\gamma$ polymorph was also consistent with molecules where long isotactic sequences were joined by either much less stereoregular blocks or short junctions with less stereoregular sequences.

The defect microstructures, resulting from any of the two-state statistical models, are inconsistent with the

observed linear growth rates. They all lead to a mixture of random crystallizable components with progressively decreasing defect contents as the molar masses increase as shown by the *C1*/CE1 sequence distributions given in Figure 3. The crystallization of these random "copolymers" is a function of the sequence propagation probability that is predicted to decrease from the highest to the lowest molar mass fraction. The more defective lower mass chains, predicted by two-state models, should present lower crystallization rates.

It is only the three-state models that meet at least some of the requirements for the crystallization behavior. The invariance in $P_0$ for the Es/*C1*/CE model for the various fractions is consistent with the experimental spherulitic linear growth rates. A difficulty with this model is the predicted predominantly syndiotactic and lowly isotactic components that are not expected to exist in the high molar mass fractions. The Es/*C1*/CE model also predicts an appreciable amount of the *C1* component with its shorter sequence lengths that is expected to yield a corresponding amount of the $\gamma$ polymorph, which was very low in these Ziegler−Natta fractions.[14]

The Es/*C1*/CE1 model yields a distribution of microstructures that is the most consistent with both the crystallization and fractionation behavior. The extremely isotactic Es component, present in all of the fractions, will be the first to crystallize at any fixed undercooling. The Es molecules in each fraction have a similar sequence propagation probability, which would confer a similar crystallization behavior to the fractions. The increasing concentration of the somewhat more defected, but still highly isotactic CE1 component with decreasing molar mass should lead to some dilution effect on the crystallization of the Es component, especially for the lower molar mass fractions. However, as found in other studies,[28,29] this effect is predicted to be low in blends of two highly isotactic components. It is also perhaps compensated by differences in molar mass and by a high degree of cocrystallization between the overlapping sequences of the distributions of the Es and CE1 components, especially among the longest sequences (see Figure 1c).

The sequence length distributions, predicted by the Es/*C1*/CE1 model, are also consistent with the formation of low contents of the $\gamma$ polymorph in all of the ZN fractions. The concentration of short crystallizable sequences, required to form this polymorph, is rather small. Most of the predicted crystallizable sequence lengths are over 200 isotactic units in agreement with the small contents of the observed $\gamma$ polymorph.[14] It is also of interest that the content of the predicted Es component by the Es/*C1*/CE1 model correlates with the observed nucleation density of each fraction. The enhanced nucleation density observed in the highest molar mass fraction was associated with unmelted aggregates or ordered structures from the longest molecules.[14] In addition, these Es molecules are indeed predicted at higher concentrations in the highest molar mass fraction. The original Busico three-state model also met these nucleation requirements.

Although the growth rates are consistent with the predicted defect microstructures of the Es/*C1*/CE1 model, there is one feature, that is, the prediction of lowly isotactic molecules (*C1*) present even in the highest molar mass fractions, which do not have an obvious explanation. During fractionation, one could expect some cocrystallization between the largely overlapping long sequences of the Es and CE1 components. Conversely, with increasing pressure during fractionation, a smaller content of CE1 would cocrystallize with the molecules of the Es component, as predicted by the progression of the content of Es component in the fractions. The low molar mass chains with very short sequence lengths, such as those predicted by the *C1* component, are not expected to precipitate with the highly isotactic chains.[23] The new three-state model, although attractive and able to explain physical properties and crystallization behavior of the fractions, is still not perfect. The possibility exists that the defected short stereo sequences, predicted by the *C1* component, may actually be part of some longer molecules and distributed in a blocky fashion resembling the stereoblock model described in the first paper.[14] An $Es_1/Es_2/Es_3 \rightarrow$ CE three-state model with the third state reversibly switching from an Es to a CE state would probably accomplish this result.

## Concluding Remarks

Microstructures from two- and three-state statistical models were compared to the respective crystallization behavior for a series of fractions obtained from a supercritical fluid fractionation of a $MgCl_2$-supported Ziegler−Natta poly(propylene). Earlier two- and three-state statistical models were modified by utilizing first-order Markovian instead of Bernoullian statistics for the chain-end control component. It seems reasonable that a chain-end control polymerization should be modeled with first-order Markovian statistics because Bernoullian statistics innately imply that there is no influence by the nature of a previous monomer insertion. Independent physical property data, such as the fractionation and polymorphic behavior of each fraction and subsequent linear growth rates utilized in this study, offer invaluable assistance in selecting an appropriate model for the behavior of $MgCl_2$-supported Ziegler−Natta catalysts. The Es/*C1*/CE1 model is the most consistent with all of the data. The predicted microstructures for $MgCl_2$-supported Ziegler−Natta catalysts consist of first, a highly isotactic poly(propylene) produced by enantiomorphic site control that has very few stereodefects. The sequence length distribution curve for this highly isotactic component peaks above 1000 repeat units irrespective of molar mass with sequences that can be as long as several thousand repeat units. It is likely that this component controls the crystallization behavior. A second important component is a mainly isotactic poly(propylene) produced by chain-end control. The sequence distribution for this component peaks around 200 repeat units and has sequences up to 1000 repeat units, once again, independent of molar mass. Structurally, there is significant overlap between the long isotactic sequences for the Es and CE1 components. The structures of the stereodefects, however, of these two components are completely different. A single, isolated configurational inversion of the type 0001000 dominates the Es component. The CE1 symmetric chain component is responsible for short syndiotactic sequences connecting longer isotactic blocks. This CE1 component also contains isotactic blocks of opposite handedness as can be detected directly by the presence of the *mmrrrm* heptad and the *mmrm* pentad in $^{13}C$ NMR spectra and which is predicted by CE1 in the Es/*C1*/CE1 model. A third type of weakly isotactic, stereoblock poly(propylene) is predicted through the *C1* switching state. Varied types of stereodefects, including

syndiotactic stereodefects, are predicted with this state, but the sequence length of the syndiotactic defect is much less than that obtained with the CE1 state in the original three-state model. It is important that the *rrrrrr* defect persists with increasing molar mass. The predicted structures from CE1 satisfy this requirement. These three types of poly(propylene)s in $MgCl_2$-supported Ziegler−Natta catalysts have also been previously proposed in a TREF study by Morini et al.[4]

The highly isotactic Es component, predicted in all the fractions but in different proportions at similar defect contents, offers an excellent explanation for the observed invariance of the linear growth rates. The effect of the highly isotactic CE1 component on the crystallization of the Es component is predicted to be small and possibly compensated by differences in molar masses. In addition, most of the crystallizable sequence lengths predicted by the Es/*C1*/CE1 model are over 200 isotactic units in agreement with the observed small contents of the $\gamma$ polymorph. The model also predicts a very high Es content in the highest molar mass fraction where enhanced nucleation was also observed.

In summary, the improved Es/*C1*/CE1 statistical model predicts a defect microstructure that is more consistent with the observed physical properties of poly(propylene) than that predicted by any of the other previous models. The question should be raised as to why a *C1* state is even necessary when all that is really required by the data is two asymmetric chain states and a first-order Markovian symmetric chain state. The near equalities of ${}^1P_0$ and ${}^2P_0$ and the closeness of $P_{11}$ and $P_{21}$ essentially reduce the *C1* model to a second simple asymmetric chain state. This result explains why satisfactory fits could be obtained with the simplest two-state model. Retention of the *C1* component adds flexibility to either a two or three-state model. The experimental data will dictate the direction the model will take as seen in the results for the two- and three-state models containing a *C1* state. The present experimental data did not possess sufficient precision to distinguish between an equality vs a real difference of 10−20% between ${}^1P_0$ and ${}^2P_0$. As $^{13}C$ NMR instrumentation progresses to higher field strengths, better signal/noise and resolution will be obtained. This will remove some of the problems in the present study where the NMR sensitivity was not sufficient to test the three-state model as adequately as would be desired.

There is one indicated structural feature from the proposed three-state model that is still difficult to explain. A small amount of highly defected molecules, predicted for the highest molar mass fractions, is not expected to persist very far into the fractionation. As already stated, a future availability of more powerful NMR capabilities, very clean fractionations and more sophisticated analytical tools should lead to further improvements in a three-state model.

**Acknowledgment.** We appreciate the contributions of Professor Vincenzo Busico, who took the time to read this paper and offer helpful comments and suggestions. R.G.A. acknowledges support by the National Science Foundation Polymer Program (DMR-0094485).

## Appendix

We described the Markovian models as *two-state* and *three-state* models, as opposed to *two-site* and *three-site* models as sometimes appears in the current literature. Markovian statistics involve transitions between "states" and because Markovian statistics can be applied to other fields outside of polymer sequence distributions, we have retained the integrity of Markovian statistics for copolymers as given by its founders; see Price.[9] The behavior of copolymer sequence distributions can be described by Markovian distributions, but the relationship to catalyst *site* behavior can only be inferred.

## References and Notes

(1) Busico, V.; Corradini, P.; De Biasio, R.; Landriani, L.; Segre, A. I. *Macromolecules* **1994**, *27*, 4521.
(2) Busico, V.; Cipullo, R.; Monaco, G.; Talarico, G.; Vacatello, M.; Chadwick, J. C.; Segre, A. L.; Sudmeijer, O. *Macromolecules* **1999**, *32*, 4173.
(3) Randall, J. C. *Macromolecules* **1997**, *30*, 803.
(4) Morini, G.; Albizzati, E.; Balbontin, G.; Mingozzi, I.; Sacchi, M. C.; Forlini, F.; Tritto, I. *Macromolecules* **1996**, *29*, 5770.
(5) Paukkeri, R.; Vaananen, T.; Lehtinen, A. *Polymer* **1993**, *34*, 2488.
(6) Chûjô, R. *Kagaku* **1981** *36*, 420.
(7) Doi, Y. *Makromol. Chem., Rapid Commun.* **1982**, *3*, 635.
(8) Price, F. P. In *Markov Chains and Monte Carlo Calculations in Polymer Science*; Lowry, G. G., Ed.; Marcel Dekker: New York, 1970; Chapter 7.
(9) Price, F. P. *J. Chem. Phys.* **1962**, *36*, 209.
(10) Bovey, F. A.; Tiers, G. V. D. *J. Polym. Sci. 44*, 173.
(11) Bovey, F. A. *High-Resolution NMR of Macromolecules*; Academic Press: New York, 1972.
(12) Harwood, Chen, T.; Lin, F. In *NMR and Macromolecules*; Randall, J. C., Ed.; ACS Symposium Series 247; American Chemical Society: Washington, DC, 1984; Chapter 13.
(13) Sato, H.; Tanaka, Y. In *NMR and Macromolecules*; Randall, J. C., Ed.; ACS Symposium Series 247; American Chemical Society: Washington, DC, 1984; Chapter 12.
(14) Part 1: Alamo, R. G.; Blanco, J. A.; Agarwal, P. K.; Randall, J. C.; Mandelkern, L. *Macromolecules* **2003**, *36*, 1559.
(15) Farina, M.; Di Silvestro, G.; Terragni, A. *Macromol. Chem. Phys.* **1995**, *196*, 353.
(16) Brintzinger, H. H.; Fischer, D.; Mülhaupt, R.; Rieger, B.; Waymouth, R. M. *Angew. Chem., Int. Ed. Engl.* **1995**, *34*, 1143.
(17) Cheng, H. N.; Kasehagen, L. J. *Macromolecules* **1993**, *26*, 4774.
(18) Ross, J. F. *J. Macromol. Sci.—Chem. Phys.* **1984**, *A21* (4), 453.
(19) Cozewith, C. *Macromolecules* **1987**, *20*, 1237.
(20) Van der Burg, M. W.; Chadwick, J. C.; Sudmeijer, O.; Tulleken, H. J. A. F. *Makromol. Chem., Theory Simul.* **1993**, *2*, 399.
(21) Coleman, B. D.; Fox, T. G. *J. Chem. Phys.* **1963**, *38*, 1065.
(22) Randall, J. C. *J. Polym. Sci., Part A: Polym. Chem.* **1998**, *36*, 1527.
(23) Flory, P. J. *Trans. Faraday Soc.* **1955**, *51*, 848.
(24) Busico, V.; Cipullo, R.; Monaco, G.; Vacatello, M.; Segre, A. L. *Macromolecules* **1997**, *30*, 6251.
(25) Arman, E. J.; Cosee, P. *J. Catal.* **1964**, *3*, 99.
(26) Ewen, J. A. *J. Am. Chem. Soc.* **1984**, *106*, 6355.
(27) Chadwick, J. C.; van Kessel, G. M. M.; Sudmeijer, O. *Macromol. Chem. Phys.* **1995**, *196*, 1431.
(28) Galante, M. J.; Mandelkern, L.; Alamo, R. G. *Polymer* **1998**, *39*, 5105.
(29) Kim, M. H.; Alamo, R. G.; Lin, J. S. *Polym. Eng. Sci.* **1999**, *39*, 2117.

MA021550F